IET Power Electronics

Research Article

IET Journals
The Institution of Engineering and Technology

Improvised predictive torque control strategy for an open end winding induction motor drive fed with four-level inversion using normalised weighted sum model

ISSN 1755-4535
Received on 18th August 2017
Revised 3rd November 2017
Accepted on 17th December 2017
E-First on 12th February 2018
doi: 10.1049/iet-pel.2017.0594
www.ietdl.org

Venkata Praveen Kumar Kunisetti[1] ✉, *Ravi Eswar Kodumur Meesala*[1], *Vinay Kumar Thippiripati*[1]

[1]*Department of Electrical Engineering, National Institute of Technology Warangal, Warangal, India*

✉ *E-mail: kvpraveenkumar15@gmail.com*

Abstract: Open end winding induction motor (OEWIM) drives are better alternate for multi-level inverter fed induction motor drives. OEWIM drives can be used in industries and electric vehicles but they entail ripple-free torque. Predictive torque control (PTC) strategy offers high dynamic performance and lesser ripple in torque, flux when compared with direct torque control. Classical PTC involves high switching frequencies and empirical methods to select weighting factors. The selection and tuning of weighting factors are cumbersome. In this article, a new normalised weighted sum model (WSM) based PTC of four-level inverter fed OEWIM is introduced to curtail torque, flux ripples, switching frequency and enhance the selection of weighting factors. The proposed algorithm uses multi-objective cost function and the optimisation of cost function is performed by using normalised WSM. The normalisation of individual cost function simplifies the selection of weighting factors to select optimal voltage vector. As a result, the proposed PTC offers all the features of classical PTC and overcomes the difficulties involved in classical PTC. Simulation and experimental studies are performed on dual inverter fed OEWIM with four-level inversion. The effectiveness of proposed algorithm is verified by comparing proposed PTC algorithm with classical PTC algorithm.

1 Introduction

High dynamic performance of variable speed drives can be obtained by using direct torque control (DTC). DTC became viable and feasible algorithm to control torque and flux of variable frequency drives (VFDs). The scheme DTC was initially developed for three-phase, two-level induction motor drives to achieve high dynamic performance [1, 2]. The limitations in DTC are: inherent ripples in torque and flux, Variable switching frequency and sluggish response at low speeds [3]. To dodge, some of the problems associated with classical DTC finite control set predictive torque control (FCS-PTC) scheme was introduced. FCS-PTC has several advantages: discrete model of inverter, discrete model of open end winding induction motor (OEWIM), does not need modulator, easy to implement, easy to understand and constraints can be added into cost function [4]. Predictive torque control (PTC) offers the features of DTC and precise steady-state performance. Implementation of PTC was introduced in [5], and it uses state-space model. Classical PTC has several challenges: it uses search algorithm to select optimum voltage vector, switching frequency is variable, higher amount of computational burden and limited prediction horizon [6]. In recent past, there is vast research has been carried in the area of FCS-PTC and applied in wider range of applications for VFDs. Dead-beat control strategy reduces computational burden, but torque ripples are dominant [7]. In [8, 9], implementation and analysis of predictive torque control scheme was implemented with hysteresis-based DTC solutions, to reduce torque and flux ripples. In [8], switching frequency-based predictive torque control was implemented but it involves high torque ripple.

The torque and flux ripple in classical PTC is high, since the selected active voltage vector is applied for whole sampling time. To trim-down torque and flux ripple duty cycle control was implemented [10]. In [11], variable switching time point-based PTC algorithm was introduced to reduce torque and flux ripples. The calculation of variable switching time point needs complex equations. In [12], novel two-vector-based PTC of induction motor was implemented to reduce torque and flux ripples. Generalised PTC (GPTC) was implemented to overcome the difficulties of duty-cycle controlled PTC [13]. GPTC can reduce torque and flux ripples but it increases computational burden. Torque of induction motor can be controlled by controlling angle between stator current and rotor flux [14]. This method introduces application of PTC for field-oriented control (FOC) by decoupling stator flux linkages.

The formulation of cost function is always chosen to track reference in classical PTC, whereas in present trends in addition to torque and flux control balancing of neutral voltage potential [15] and reduction of common-mode voltage [16] are added in cost function for multi-level inverter fed induction motor drives. The minimisation of cost function is achieved by tuning the weighting factors involved in the cost function. There is no particular method to select the weighting factors, some of researcher's used branch and bound algorithm to select the weighting factors [6, 17]. In [18], selection of flux weighting factor is given by ratio of rated torque and flux, for real –time implementation further tuning is required. In [12], weighting factors was eliminated by converting torque and flux reference into equivalent flux space vector. Multi-objective ranking-based PTC algorithm was implemented to eliminate weighting factor selection [19], but it involves large computations when compared to classical PTC. In [20], sugeno-fuzzy method was introduced to select weighting factors with online optimisation.

Based on the literature, the challenges in FCS-PTC are: variable switching frequency, tedious tuning of weighting factors and higher ripples. In order to abate these limitations duty-cycle control, dead-beat control and multi-level inverter fed induction motor drives are implemented. In this article, an attempt is made to reduce switching frequency, torque and flux ripples by using multi-level inverter fed OEWIM configuration. OEWIM is an attractive alternate for multi-level inverters. OEWIM has various features, when compared with other multi-level inverter topologies [21]. OEWIM shows its strength in the applications such as electric vehicles [22, 23], renewable energy integration [24–26] and ship propulsion [27]. OEWIM with dual two-level voltage source inverter (VSI) can provide two-, three- and four-level inversion. If two-level VSIs are replaced by neutral point clamped three-level inverter, it is also possible to extend the output voltage for more than four-level inversion [28] with less number of switches. These adorable features of OEWIM embark to the implementation of

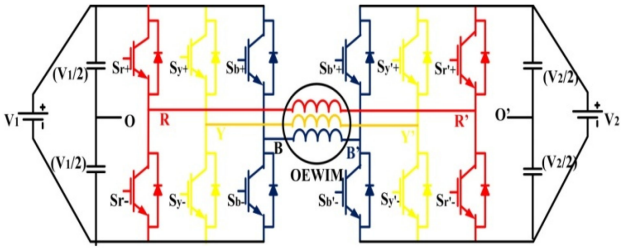

Fig. 1 *Four-level inverter fed OEWIM*

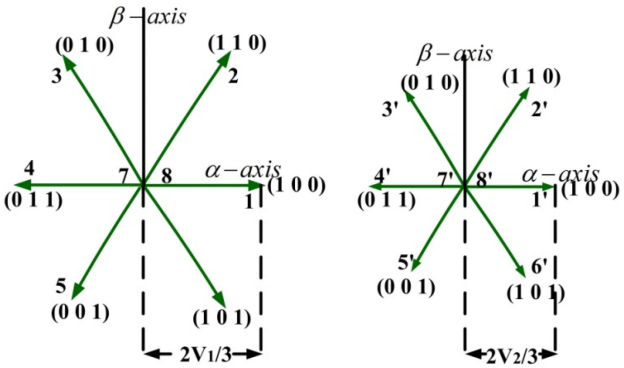

Fig. 2 *Location of space vectors for VSI-1 and VSI-2*

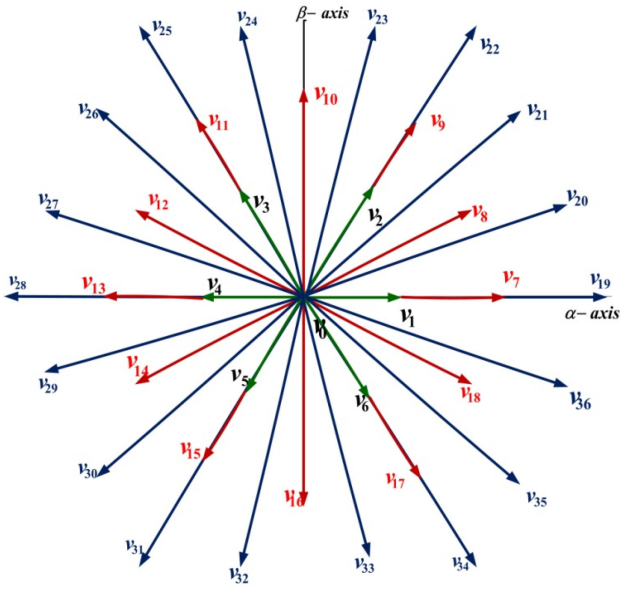

Fig. 3 *Resultant voltage space vectors of dual inverter configuration*

proposed algorithm. To extend the applications of OEWIM drives, it is necessary to obtain ripple-free torque for VFDs. Ripple-free torque can be obtained by using FOC or DTC. In [29], DTC of OEWIM was implemented with two-level inversion and it describes the realisation of switching states. Space vector modulated DTC (SVM-DTC) of OEWIM was implemented to reduce torque ripple [30]. The calculation of reference voltage space vector plays a vital role in SVM-DTC and it is quite complex. In [29, 30], two VSIs are energised with same magnitude of DC voltage, so [29] gives the DTC of OEWIM for two-level inversion and [30] demonstrates SVM-DTC of OEWIM. Predictive torque control of OEWIM drive with multi-level inversion was introduced [31]. In [32], PTC of OEWIM was implemented with three-level inversion and it uses limited number of switching states to reduce zero-sequence currents, it increases torque ripple.

This article describes the implementation of predictive torque controlled OEWIM with four-level inversion. Four-level configuration of OEWIM was obtained by operating two VSIs with unequal DC voltages [33]. In this article, normalised weighted sum model (WSM) is introduced to optimise the cost function. WSM is a multi-criteria decision-making algorithm and it is easy to implement [34, 35]. Intentions of this article are: implementing discrete model of OEWIM, inverter with finite number of switching states, enhanced selection of weighting factors, formulation of cost function to reduce ripples (torque and flux) and reduction of switching frequency. The effectiveness of proposed PTC algorithm was verified by implementing with SIMULINK and experimentation. The experimentation was carried by implementing the proposed algorithm with dSPACE DS-1104 controller.

2 Discrete model of dual inverter fed OEWIM

Power circuit configuration of four-level inverter fed OEWIM is shown in Fig. 1. It consists of an OEWIM driven by 2 two-level VSIs with unequal DC-link voltages. Two VSIs are operated with the voltage $V_1 = 2V_{dc}/3$ and $V_2 = V_{dc}/3$. The two inverters are operated with isolated DC sources and the net voltage presenting at the terminals of OEWIM is 'V_{dc}= V_1+V_2'. In Fig. 2, (1–8) represents voltage space vectors of VSI-1 and (1′–8′) represents voltage space vectors of VSI-2. Two-level VSI develops '8' switching states, the combination of two inverters develops (8 × 8) space vector locations. Out of these '64' voltage space vector locations, it gives 37 active voltage vectors. The location of '37' active voltage vectors is shown in Fig. 3.

The resultant voltage space vector (3) was obtained by using (1) and (2). Output voltage of VSI-1 is given by (1), whereas (2) gives output voltage of VSI-2

$$V_{s1} = (2/3)(V_1)\left(S_r + S_y e^{j2\pi/3} + S_b e^{j4\pi/3}\right) \quad (1)$$

$$V_{s2} = (2/3)(V_2)\left(S'_r + S'_y e^{j2\pi/3} + S'_b e^{j4\pi/3}\right) \quad (2)$$

$$V_s = V_{s1} - V_{s2} \quad (3)$$

In (3), V_{s1} indicates voltage space vector of VSI-1, V_{s2} indicates voltage space vector of VSI-2 and V_s indicates resultant voltage space vector of dual-inverter.

Locations of active voltage space vector (v_0–v_{36}) were shown in Fig. 3. The resultant voltage space vector (3) was evaluated by considering all possible switching states of VSI-1 and VSI-2.

2.1 Dynamic model of dual inverter configuration

The pole voltages of VSI-1 are named as V_{ro}, V_{yo} and V_{bo}. The pole voltages of VSI-2 are named as $V_{r'o'}$, $V_{y'o'}$ and $V_{b'o}$ ′ The pole voltage of inverter-1 'V_{ro}' assumes $V_{dc}/3$ or $-V_{dc}/3$, similarly the pole voltage of inverter-2 '$V_{r'o}$' is $V_{dc}/6$ or $-V_{dc}/6$ [21]. The phase voltages of OEWIM are obtained from common mode voltage and difference of pole voltages

$$\begin{bmatrix} V_{ro} \\ V_{yo} \\ V_{bo} \end{bmatrix} = \begin{cases} \frac{V_{dc}}{3} \text{ when } S_r = S_y = S_b = 1 \\ -\frac{V_{dc}}{3} \text{ when } S_r = S_y = S_b = 0 \end{cases} \quad (4)$$

$$\begin{bmatrix} V_{r'o'} \\ V_{y'o'} \\ V_{b'o'} \end{bmatrix} = \begin{cases} \frac{V_{dc}}{6} \text{ when } S_{r'} = S_{y'} = S_{b'} = 1 \\ -\frac{V_{dc}}{6} \text{ when } S'_r = S'_y = S_{b'} = 0 \end{cases} \quad (5)$$

The difference of pole voltages is given by (6). Pole voltages of VSI-1 are given by (4) and pole voltages of VSI-2 are given by (5). In (4) and (5), if S_r to $S_{b'} = 1$ then top switch of respective leg is ON similarly when S_r to $S_{b'} = 0$ bottom switch of respective leg is ON

$$\begin{bmatrix}\Delta V_{rr'}\\ \Delta V_{yy'}\\ \Delta V_{bb'}\end{bmatrix}=\begin{bmatrix}V_{ro}-V_{r'o'}\\ V_{yo}-V_{y'o'}\\ V_{bo}-V_{b'o'}\end{bmatrix} \tag{6}$$

Zero-sequence voltage of OEWIM is given by (7) and it is obtained from difference of pole voltages

$$V_{oo'}=(1/3)\left(\Delta V_{rr'}+\Delta V_{yy'}+\Delta V_{bb'}\right) \tag{7}$$

The phase voltages of OEWIM were obtained by assuming the points 'o' and 'o'' are shorted [21]. The phase voltages of OEWIM were given as

$$\begin{bmatrix}V_{rr'}\\ V_{yy'}\\ V_{bb'}\end{bmatrix}=\begin{bmatrix}\Delta V_{rr'}\\ \Delta V_{yy'}\\ \Delta V_{bb'}\end{bmatrix}-\begin{bmatrix}V_{oo'}\\ V_{oo'}\\ V_{oo'}\end{bmatrix} \tag{8}$$

From (8), the simplified inverter model in terms of pole voltages of VSI-1 and VSI-2 can be written as

$$\begin{bmatrix}V_{rr'}\\ V_{yy'}\\ V_{bb'}\end{bmatrix}=(1/3)\begin{bmatrix}2&-1&-1\\ -1&2&-1\\ -1&-1&2\end{bmatrix}\begin{bmatrix}\Delta V_{rr'}\\ \Delta V_{yy'}\\ \Delta V_{bb'}\end{bmatrix} \tag{9}$$

2.2 Discrete model of OEWIM

Discrete model of OEWIM is implemented in stationary reference frame. Stator and rotor voltages of OEWIM in stationary reference frames are given by (10) and (11). The voltage equations of stator and rotor are obtained by applying abc-αβ transformation [36].

$$\begin{bmatrix}V_{s\alpha}(k)\\ V_{s\beta}(k)\end{bmatrix}_m=R_s\begin{bmatrix}i_{s\alpha}(k)\\ i_{s\beta}(k)\end{bmatrix}_m+p\begin{bmatrix}\psi_{s\alpha}(k)\\ \psi_{s\beta}(k)\end{bmatrix}_m \tag{10}$$

$$\begin{bmatrix}0\\ 0\end{bmatrix}=R_r\begin{bmatrix}i_{r\alpha}(k)\\ i_{r\beta}(k)\end{bmatrix}_m+p\begin{bmatrix}\psi_{r\alpha}(k)\\ \psi_{r\beta}(k)\end{bmatrix}_m+\omega_r\begin{bmatrix}\psi_{r\beta}(k)\\ -\psi_{r\alpha}(k)\end{bmatrix}_m \tag{11}$$

where 'p' is d/dt.

Flux linkages of stator and rotor are given by (12) and (13), (14) represents magnitude of stator flux space vector [4]

$$\begin{bmatrix}\psi_{s\alpha}(k)\\ \psi_{s\beta}(k)\end{bmatrix}_m=L_s\begin{bmatrix}i_{s\alpha}(k)\\ i_{s\beta}(k)\end{bmatrix}_m+L_m\begin{bmatrix}i_{r\alpha}(k)\\ i_{r\beta}(k)\end{bmatrix}_m \tag{12}$$

$$\begin{bmatrix}\psi_{r\alpha}(k)\\ \psi_{r\beta}(k)\end{bmatrix}_m=L_r\begin{bmatrix}i_{r\alpha}(k)\\ i_{r\beta}(k)\end{bmatrix}_m+L_m\begin{bmatrix}i_{s\alpha}(k)\\ i_{s\beta}(k)\end{bmatrix}_m \tag{13}$$

$$(\psi_s(k))_m=\left|\psi_{s\alpha}(k)+\mathrm{j}\psi_{s\beta}(k)\right|=\left|\psi_s(k)\right|_m \tag{14}$$

Torque (15) of OEWIM is given as[36]

$$T(k)_m=(3/2)(P/2)\left(\psi_{s\alpha}(k)_m i_{s\beta}(k)_m-\psi_{s\beta}(k)_m i_{s\alpha}(k)_m\right) \tag{15}$$

Speed of OEWIM is obtained from state-space model

$$\begin{cases}T(k)_m-T_L=J(p\omega_m)+B\omega_m\\ (p\omega_m)=\dfrac{1}{J}(T(k)_m-T_L-B\omega_m)\end{cases} \tag{16}$$

3 Proposed PTC strategy

3.1 Classical PTC

Classical FCS-PTC of OEWIM can be implemented by using following steps: (i) implementing the dynamic model of VSI to identify all possible switching states, (ii) implementing discrete model of OEWIM to identify control variables, (iii) measure the variables (speed and current) required for prediction, (iv) estimate the non-measurable variables (flux and torque) at kth instant, (v) predict the control variables for all possible switching combinations, (vi) implementing the cost function and (vii) minimisation of cost function to generate switching pulses.

3.1.1 Prediction of control variables: The control variables in classical PTC are torque and flux. To predict control variables forward Euler method (17) and (18) is used. The control variables are predicted for '37' possible switching states of OEWIM. The state-space model of OEWIM is used to predict torque and flux of OEWIM by predicting stator current

$$\frac{\mathrm{d}x}{\mathrm{d}t}=\frac{x(k+1)-x(k)}{T_s} \tag{17}$$

$$x(k+1)=(\mathrm{d}x/\mathrm{d}t)T_s+x(k) \tag{18}$$

The state-space equations of stator flux are obtained by using (10), the estimation of stator flux is shown in Appendix in Section 6

$$p\begin{bmatrix}\psi_{s\alpha}(k)\\ \psi_{s\beta}(k)\end{bmatrix}_m=\begin{bmatrix}V_{s\alpha}(k)\\ V_{s\beta}(k)\end{bmatrix}_m-R_s\begin{bmatrix}i_{s\alpha}(k)\\ i_{s\beta}(k)\end{bmatrix}_m \tag{19}$$

From (19), stator flux can be predicted as

$$\begin{bmatrix}\psi_{s\alpha}(k+1)\\ \psi_{s\beta}(k+1)\end{bmatrix}_m=T_s\left(\begin{bmatrix}V_{s\alpha}(k)\\ V_{s\beta}(k)\end{bmatrix}_m-R_s\begin{bmatrix}i_{s\alpha}(k)\\ i_{s\beta}(k)\end{bmatrix}_m\right)+\begin{bmatrix}\psi_{s\alpha}(k)\\ \psi_{s\beta}(k)\end{bmatrix}_m \tag{20}$$

The simplified state-space equations of stator current are derived from (10) to (13)

$$p\begin{bmatrix}i_{s\alpha}(k)\\ i_{s\beta}(k)\end{bmatrix}_m=C\begin{bmatrix}A\begin{bmatrix}\psi_{s\alpha}(k)\\ \psi_{s\beta}(k)\end{bmatrix}_m-E\begin{bmatrix}i_{s\alpha}(k)\\ i_{s\beta}(k)\end{bmatrix}_m+B\begin{bmatrix}\psi_{s\beta}(k)\\ -\psi_{s\alpha}(k)\end{bmatrix}_m\\ -D\begin{bmatrix}i_{s\beta}(k)\\ i_{s\alpha}(k)\end{bmatrix}_m+F\begin{bmatrix}V_{s\alpha}(k)\\ V_{s\beta}(k)\end{bmatrix}_m\end{bmatrix} \tag{21}$$

Stator currents can be predicted from (21) and it is given by

$$\begin{bmatrix}i_{s\alpha}(k+1)\\ i_{s\beta}(k+1)\end{bmatrix}_m=T_s\left(C\begin{bmatrix}A\begin{bmatrix}\psi_{s\alpha}(k)\\ \psi_{s\beta}(k)\end{bmatrix}_m-E\begin{bmatrix}i_{s\alpha}(k)\\ i_{s\beta}(k)\end{bmatrix}_m\\ +B\begin{bmatrix}\psi_{s\beta}(k)\\ -\psi_{s\alpha}(k)\end{bmatrix}_m\\ -D\begin{bmatrix}i_{s\beta}(k)\\ i_{s\alpha}(k)\end{bmatrix}_m+F\begin{bmatrix}V_{s\alpha}(k)\\ V_{s\beta}(k)\end{bmatrix}_m\end{bmatrix}\right)+\begin{bmatrix}i_{s\alpha}(k)\\ i_{s\beta}(k)\end{bmatrix}_m \tag{22}$$

If stator flux and current equations are known, then it is easy to predict torque of OEWIM

$$T(k+1)_m=(3/2)(P/2)\begin{pmatrix}\psi_{s\alpha}(k+1)_m i_{s\beta}(k+1)_m\\ -\psi_{s\beta}(k+1)_m i_{s\alpha}(k+1)_m\end{pmatrix} \tag{23}$$

From (20), the magnitude of predicted stator flux is given as

$$\psi_s(k+1)_m=\left|\left(\psi_{s\alpha}(k+1)_m+\mathrm{j}\psi_{s\beta}(k+1)_m\right)\right| \tag{24}$$

where $A=R_r/L_m$, $B=\omega_e(L_r/L_m)$, $C=L_m/(L_sL_r-L_m^2)$, $D=\omega_e/C$ $E=1/L_m(R_rL_s-R_sL_r)$, $F=L_r/L_m$, $m=[v_0, v_1, v_2, \ldots, v_{36}]$, '$T_s$' is sample time, '$\omega_m$' indicates mechanical rad/s and 'ω_e' indicates electrical rad/s.

3.1.2 Formulation of cost function: Selection of switching states is made by minimisation of cost function. The cost function is used to meet control law. In classical PTC, control law is defined for torque and flux. The cost function is given as

$$g=(T_{\mathrm{ref}}-T(k+1)_m)-w(\psi_{\mathrm{sref}}-\psi_s(k+1)_m) \tag{25}$$

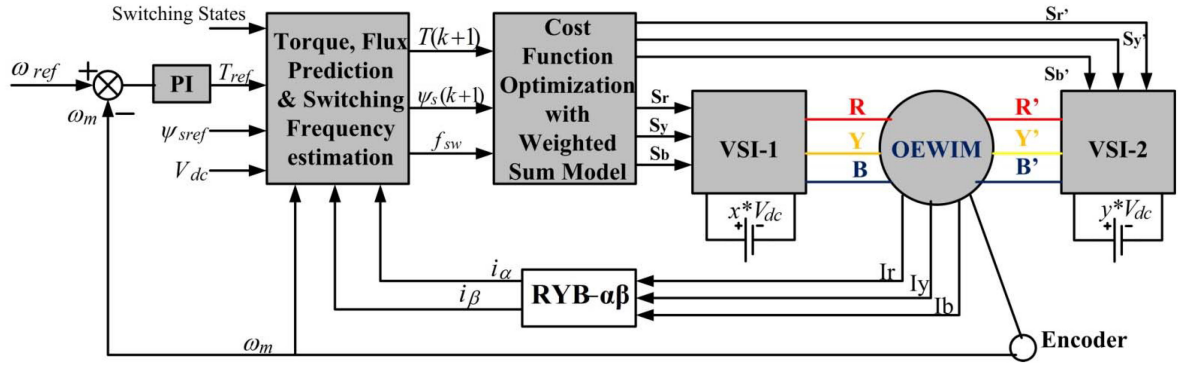

Fig. 4 *Block diagram of proposed PTC*

Cost function of classical PTC consists of two parts. First part is to reduce the torque error and second part of cost function is to minimise the flux error. In (25), 'w' indicates stator flux weighting factor. The weighting factor used in classical PTC is given as

$$w = \frac{T_{\text{nom}}}{\psi_{\text{nom}}} \tag{26}$$

where 'T_{nom}' is rated torque and 'ψ_{nom}' is rated flux. The selection of 'w' plays a vital role on the performance of OEWIM. Initially, 'w' is taken as fixed value, whereas for real-time implementation tuning of 'w' is required. Tuning of 'w' is cumbersome and tedious process. Minimisation of cost function is evaluated for all possible switching combinations of inverter. The switching frequency required in classical PTC is very high. In power converters switching frequency is a good measure. As switching frequency increases, number of commutations of power switches will increase. To limit the number of commutations switching frequency can be reduced. In order to reduce the torque and flux ripples multi-level inversion is used. The switching frequency is reduced by modifying cost function. This article uses normalised WSM to provide same performance of classical PTC along with reduction of switching frequency and an attempt to reduce tedious tuning process of weighting factors.

3.2 Proposed PTC of OEWIM using weighted sum model

Block diagram of proposed PTC strategy is shown in Fig. 4. In classical PTC cost function comprises of only two control variables. For multi-level inversion, the number of switches is more which increases commutations and causes switching losses. In order to reduce the switching frequency cost function is reframed with three control objectives. The proposed PTC algorithm is implemented by considering multi-objective cost function. If the cost function consists of multiple control objectives then it is obvious to find weighting factors associated with each and every individual control objective and the tuning of these weighting factors unavoidable. This article uses a multi-criteria decision-making algorithm to simplify the selection of weighting factors by using normalised WSM.

3.2.1 Implementation of normalised WSM: The selection of weighting factor affects the performance of OEWIM. If the cost function comprises of more than two control variables, then the selection of weighting factors is complicate. In proposed PTC algorithm, the cost function comprises of three control objectives.

The steps involved to implement proposed PTC are given below:

(i) Generate decision matrix using control objectives.
(ii) Normalise the decision matrix.
(iii) Obtain weighted normalised decision matrix.
(iv) Determine optimum voltage vector to meet control objective.

In classical PTC single cost function is used, whereas in proposed PTC multi-objective cost function is developed by separating into individual cost functions. The control objectives used in proposed PTC algorithm are given as

$$[G_1]_m = (T_{\text{ref}} - T(k+1)_m) \tag{27}$$

$$[G_2]_m = \frac{T_{\text{nom}}}{\psi_{\text{nom}}}(\psi_{s\text{ref}} - \psi_s(k+1)_m) \tag{28}$$

and

$$[G_3]_m = \frac{1}{V_{\text{dc}}}(v_s(k)_m - v_s(k+1)_m) \tag{29}$$

Four-level inverter fed OEWIM has '37' possible space vector locations (switching states). The decision matrix is developed to reduce torque ripple (27), flux ripple (28) and switching frequency reduction (29). The decision matrix is shown below. The switching frequency of an inverter depends on control effort involved to optimise the cost function. By reducing the control effort, it is possible to reduce the switching frequency. In general, the control effort is associated with voltage variations, current variations or switching losses.

In this article, the switching frequency of dual inverter configuration is controlled by reducing the number of voltage transitions

$$[D]_m = [G_1 \quad G_2 \quad G_3]_m \tag{30}$$

Normalised decision matrices are obtained from (30) and it is given by

$$[N_1]_m = \frac{[G_1]_m - \min [G_1]_m}{\max [G_1]_m - \min [G_1]_m} \tag{31}$$

$$[N_2]_m = \frac{[G_2]_m - \min [G_2]_m}{\max [G_2]_m - \min [G_2]_m} \tag{32}$$

$$[N_3]_m = \frac{[G_3]_m - \min [G_3]_m}{\max [G_3]_m - \min [G_3]_m} \tag{33}$$

By normalising the control objectives (27)–(29), their range is converted to exist in the range of 0–1.

With the help of normalised decision matrix, the cost function can be formulated by using WSM and is given as

$$G = w_1[N_1]_m + w_2[N_2]_m + w_3[N_3]_m = \sum_{i=1}^{3} w_i(N_i)_m \tag{34}$$

where $w_1 = w_2 = w_3 = (1/3)$. The weighting factors used in proposed PTC are fixed quantities; hence, tedious tuning process is eliminated.

Evaluation of cost function by using normalised WSM for one sample period is shown in Table 1. In Table 1, V_s is voltage space vector, 'G_1' is torque control law, 'G_2' is flux control law and 'G_3'

Table 1 Optimal voltage vector selection in one sample period from online simulation

Voltage space vector (V_s)	G_1	G_2	G_3	N_1	N_2	N_3	G
v_0	3.4256	0.4774	0.5879	0.4485	0.0625	0.077	0.196
v_1	4.3741	0.1618	0.7698	0.5727	0.0212	0.1008	0.231567
v_2	2.9703	0.3067	0.5879	0.3889	0.0402	0.077	0.1687
v_3	2.0218	0.3266	0.3849	0.2647	0.0428	0.0504	0.1193
v_4	2.4771	1.1128	0.444	0.3243	0.1457	0.0582	0.176067
v_5	3.8809	1.2605	0.6667	0.5082	0.1651	0.0873	0.253533
v_6	4.8294	0.6192	0.8012	0.6324	0.0811	0.1049	0.2728
v_7	5.3229	0.8048	0.9686	0.6969	0.1054	0.1268	0.3097
v_8	3.9188	0.9439	0.8012	0.5131	0.1236	0.1049	0.2472
v_9	2.5149	1.092	0.6667	0.3293	0.143	0.0873	0.186533
v_{10}	1.5664	0.4606	0.4444	0.2051	0.0603	0.0582	0.107867
v_{11}	**0.6179**	**0.1668**	**0.2222**	**0.0809**	**0.0218**	**0.0291**	**0.043933**
v_{12}	1.0732	0.956	0.2222	0.1405	0.1252	0.0291	0.098267
v_{13}	1.5286	1.7442	0.3849	0.2002	0.2284	0.0504	0.159667
v_{14}	2.9324	1.8979	0.5879	0.384	0.2485	0.077	0.2365
v_{15}	4.3363	2.0425	0.8012	0.5678	0.2674	0.1049	0.313367
v_{16}	5.2848	1.3991	0.8889	0.692	0.1832	0.1164	0.330533
v_{17}	6.2333	0.752	1.0184	0.8162	0.0985	0.1333	0.349333
v_{18}	5.7779	0.0258	0.9686	0.7566	0.0034	0.1268	0.2956
v_{19}	6.2711	1.4515	1.1759	0.8211	0.1901	0.154	0.3884
v_{20}	4.8673	1.5849	1.0184	0.6373	0.2075	0.1333	0.326033
v_{21}	3.4634	1.7272	0.8889	0.4535	0.2262	0.1164	0.265367
v_{22}	2.0596	1.8782	0.8012	0.2697	0.2459	0.1049	0.206833
v_{23}	1.1111	1.2488	0.5879	0.1455	0.1635	0.077	0.128667
v_{24}	0.1626	0.6233	0.3849	0.0213	0.0816	0.0504	0.0511
v_{25}	0.7859	0.0019	0.2222	0.1029	0.0003	0.0291	0.0441
v_{26}	0.3306	0.7901	0	0.0433	0.1035	0	0.048933
v_{27}	0.1247	1.5813	0.2222	0.0163	0.2071	0.0291	0.084167
v_{28}	0.5801	2.3715	0.4444	0.076	0.3105	0.0582	0.148233
v_{29}	1.9839	2.5314	0.5879	0.2598	0.3315	0.077	0.222767
v_{30}	3.3877	2.682	0.7698	0.4436	0.3512	0.1008	0.298533
v_{31}	4.7916	2.8233	0.9686	0.6274	0.3697	0.1268	0.374633
v_{32}	5.7401	2.1778	1.0184	0.7516	0.2852	0.1333	0.390033
v_{33}	6.6886	1.5285	1.1111	0.8758	0.2001	0.1455	0.407133
v_{34}	7.6371	0.8755	1.2373	1	0.1146	0.162	0.425533
v_{35}	7.1818	0.1011	1.1759	0.9404	0.0132	0.154	0.3692
v_{36}	6.7265	0.6746	1.1547	0.8808	0.0883	0.1512	0.373433

is control law to reduce switching frequency. From the control performance, 'v_{11}' gives minimum ripple in torque, flux and less switching frequency during one sample time. For example, in one sampling interval G_3 is obtained by using voltage space vectors at kth and $k+1$ state. Let us suppose, the voltage space vector applied at kth and $(k+1)$ instant are V_{11} and V_{25}. Then G_3 from (29) is 0.222. Table 1 is obtained by implementing the proposed PTC in MATLAB, while running the online simulation the data has been collected for individual cost functions over one sampling interval. Table 1 is an example of individual cost function evaluated for all 37 possible combinations. Out of these switching combinations, the switching state which provides minimum value of cost function is selected as optimal voltage vector. The selected voltage vector is applied to dual inverter fed OEWIM configuration.

The cost function (34) uses multi-objective function, so the proposed PTC strategy can reduce ripples in torque, flux and also switching frequency. The switching frequency of OEWIM can be reduced by number of voltage vector transitions.

4 Simulation and experimental results

After implementing dynamic models of VSI and OEWIM, the proposed PTC algorithm is tested by implementing it in SIMULINK. The parameters used to implement the proposed algorithms are shown in Appendix. Figs. 5–10 demonstrate simulation and experimental results of classical and proposed PTC algorithms.

The four-level inversion is obtained by operating the two VSIs with unequal DC voltages (2:1 ratio). The two VSIs are operated with the voltages of 380 and 160 V. Hence, the effective DC voltage is 540 V. The proposed PTC algorithm was tested at various operating conditions. In interest of brevity, the results of classical and proposed PTC algorithms are described for 100 and 125 rad/s. The simulation and experimental results are shown for forward and reverse motoring modes. Fig. 5 describes speed, torque and flux of OEWIM drive when a step change in speed applied from 125 to −125 rad/s (forward motoring to reverse motoring). Figs. 5*a* and *b* present simulated and experimental results of classical PTC for step change in speed from forward motoring to reverse motoring. Figs. 5*c* and *d* present simulated and experimental results of proposed PTC for step change in speed from forward motoring to reverse motoring. From Fig. 5, it is

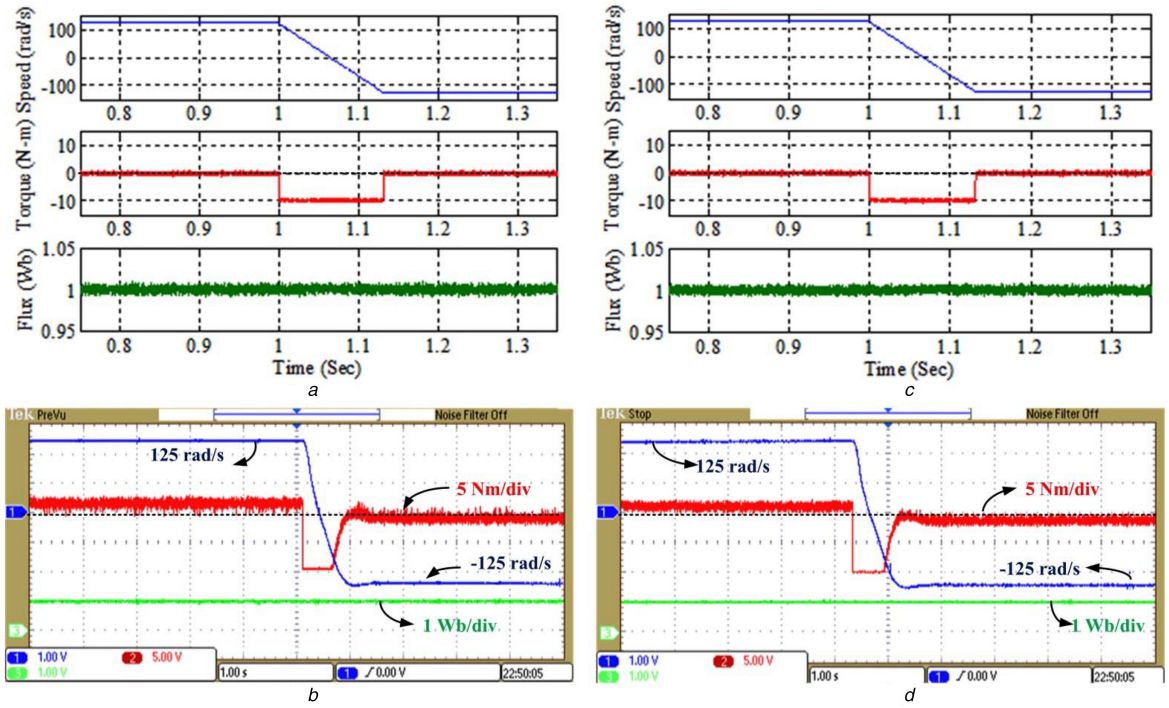

Fig. 5 *Forward and reverse motoring of dual inverter fed OEWIM*
(a) Simulated response of classical PTC, ***(b)*** Experimental response of classical PTC, ***(c)*** Simulated response of proposed PTC, ***(d)*** Experimental response of proposed PTC

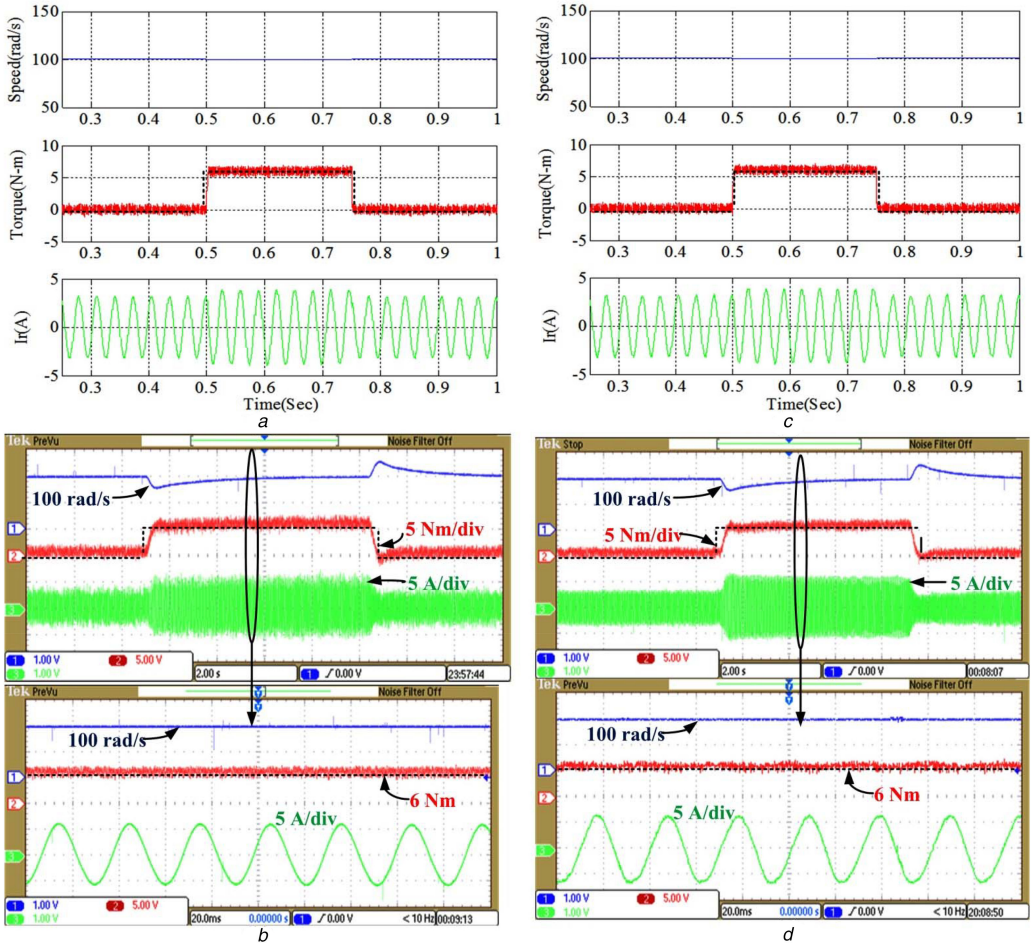

Fig. 6 *Forward motoring of OEWIM for a load torque of 6 N m at 100 rad/s*
(a) Simulated response of classical PTC, ***(b)*** Experimental response of classical PTC (top-dynamic variation of load, bottom-zoomed portion), ***(c)*** Simulated response of proposed PTC and, ***(d)*** Experimental response of proposed PTC (top-dynamic variation of load, bottom-zoomed portion)

evident that the proposed PTC gives all the features of classical PTC in addition it reduces a little amount of torque and flux ripples. Fig. 6 describes speed, torque and R-Phase current of OEWIM drive in forward motoring at a steady speed of 100 rad/s and a load torque of 6 N m. Figs. 6*a* and *b* present simulated and experimental results of classical PTC for forward motoring.

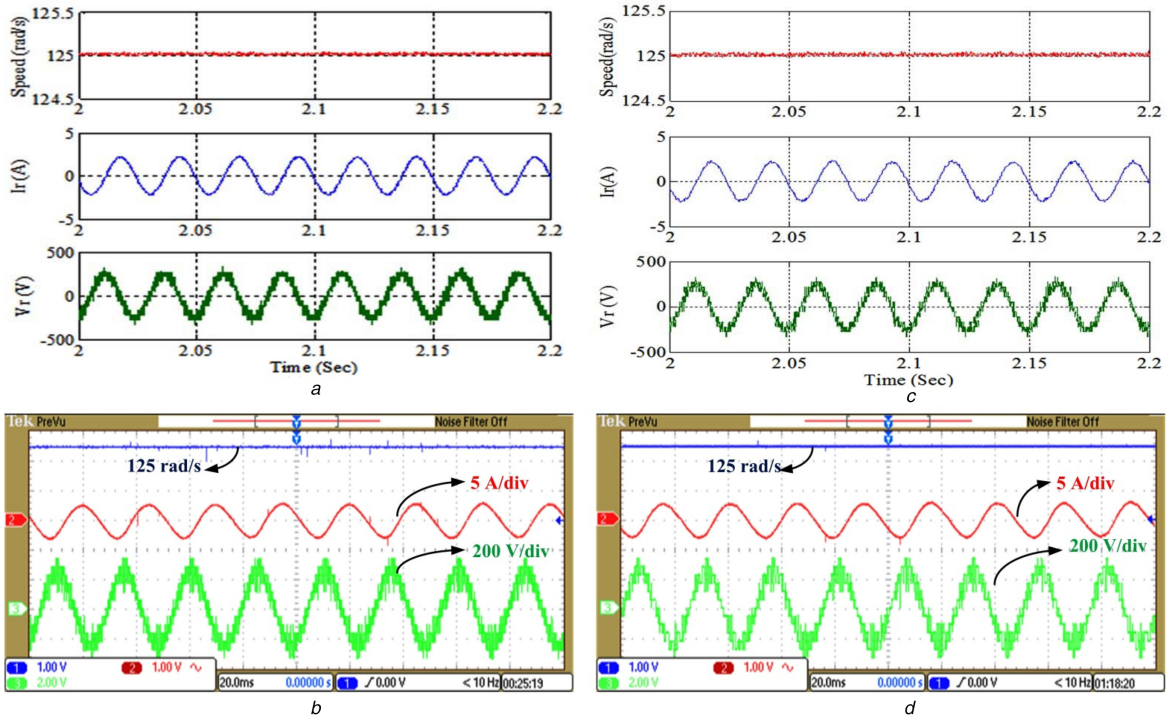

Fig. 7 *Steady-state speed, current and voltage of dual inverter fed OEWIM*
(a) Simulated response of classical PTC, ***(b)*** Experimental response of classical PTC, ***(c)*** Simulated response of proposed PTC, ***(d)*** Experimental response of proposed PTC

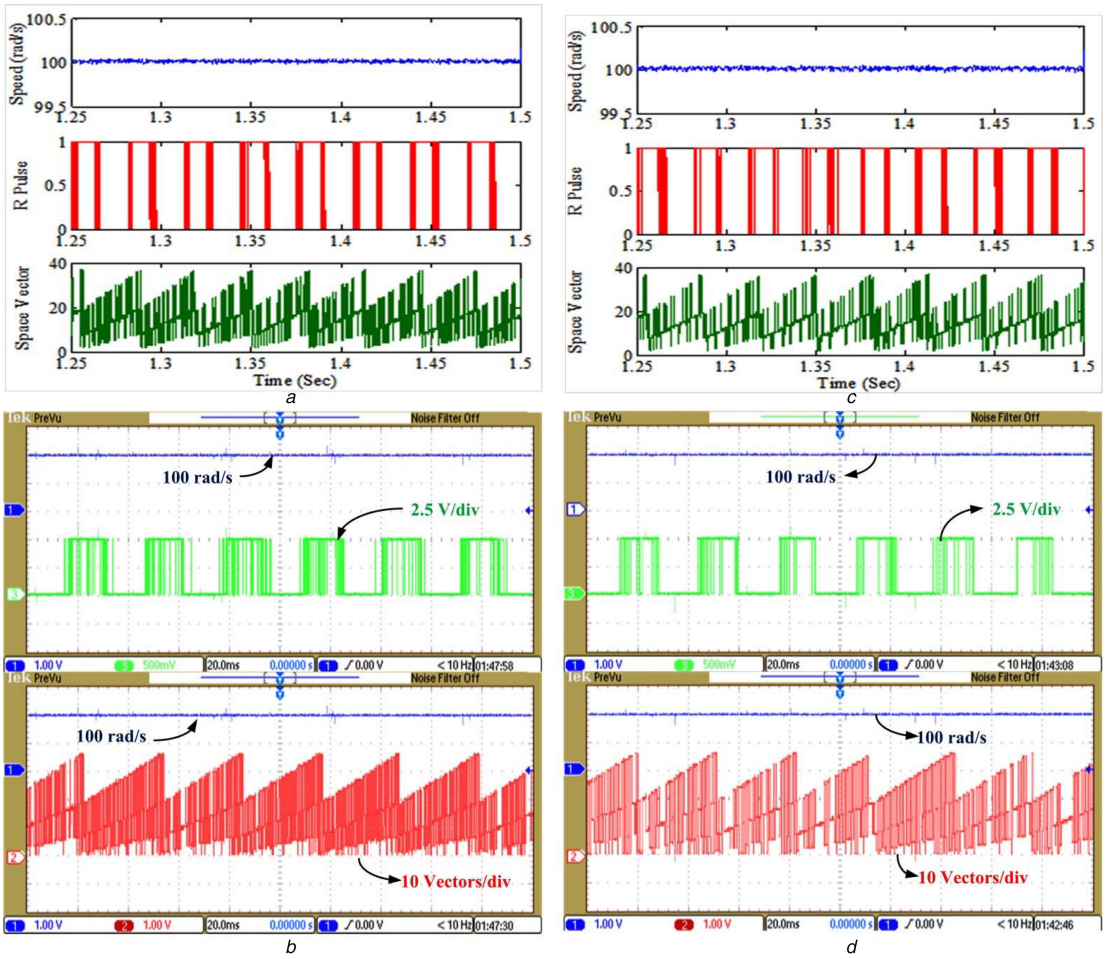

Fig. 8 *Steady-state speed, switching pulse of R-phase and selected voltage vector of four-level inverter fed OEWIM drive*
(a) Simulated response of classical PTC, ***(b)*** Experimental response of classical PTC, ***(c)*** Simulated response of proposed PTC, ***(d)*** Experimental response of proposed PTC

Figs. 6*c* and *d* present simulated and experimental results of proposed PTC in forward motoring. In Figs. 5 and 6, black-dashed line indicates reference torque. Fig. 7 demonstrates speed, current and voltage of OEWIM drive at a steady speed of 125 rad/s. Figs. 7*a* and *b* present simulated and experimental results of classical PTC, whereas Figs. 7*c* and *d* present simulated and

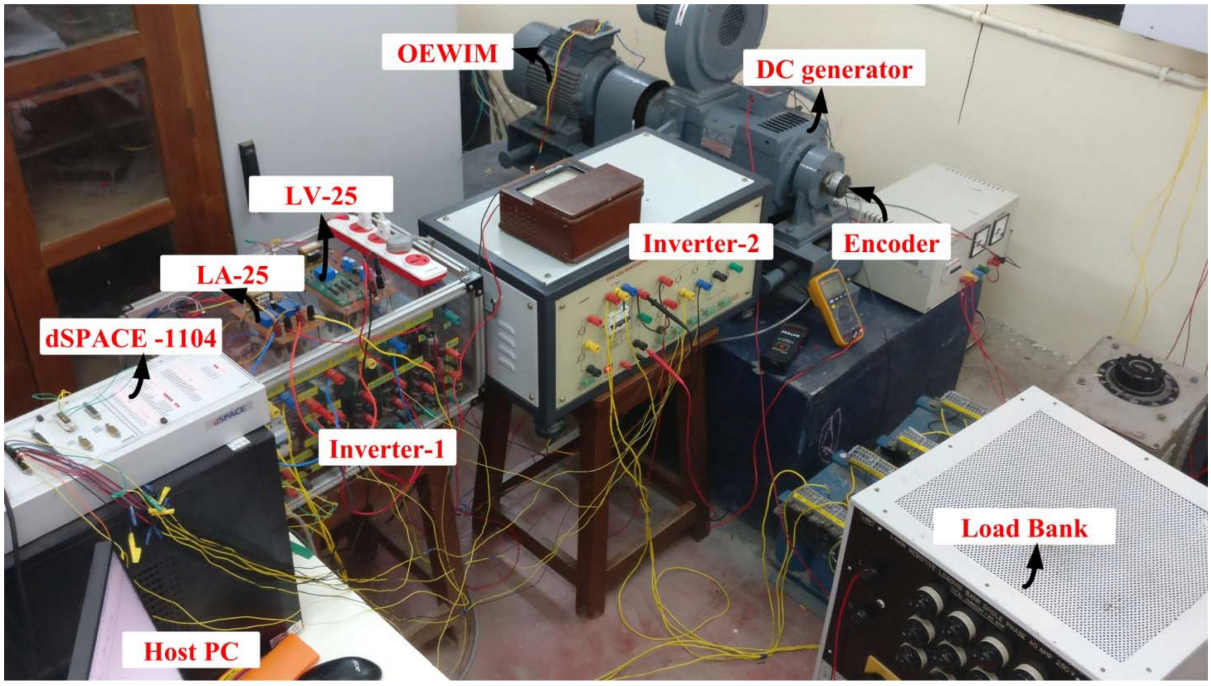

Fig. 9 *Test-rig used for experimental verification*

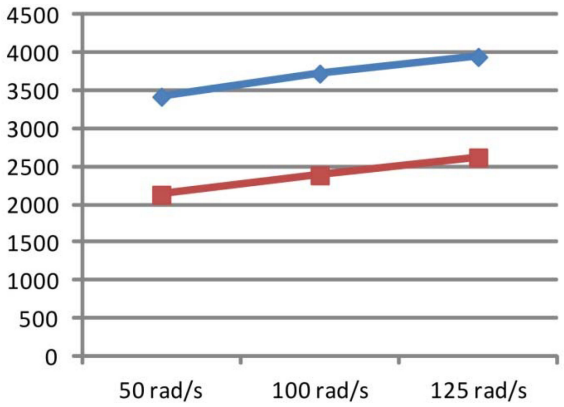

Fig. 10 *Switching frequency involved in classical (blue) and proposed PTC (red)*

Table 2 Steady-state torque, flux ripple and switching frequency of OEWIM drive for various speeds of operation

Control scheme	Speed, rad/s	Torque ripple, N m	Flux ripple, Wb	Switching frequency, Hz
classical PTC	50	2.8	0.025	3423
proposed PTC		2.5	0.022	2131
classical PTC	100	2.2	0.016	3727
proposed PTC		2.0	0.015	2388
classical PTC	125	1.4	0.012	3947
proposed PTC		1.25	0.01	2622

experimental results of proposed PTC. From Fig. 7, it is observed that the proposed PTC can reduce switching frequency. Fig. 8 describes speed, R-phase pulse and selection of optimum voltage vector at a steady speed of 100 rad/s. Figs. 8*a* and *b* present simulated and experimental results of classical PTC, whereas Fig. 8*c* and *d* represent simulated and experimental results of proposed PTC. From Fig. 8, it is clear that proposed PTC operates with lower switching frequencies. Test bench used to implement proposed algorithm for experimentation is shown in Fig. 9. The implementation of PTC algorithm requires an incremental encoder to sense the speed, a voltage sensor, and two current sensors. The output of theses sensors is given to analogue-to-digital converters of dSPACE controller. Switching frequency (Hz) involved in classical and proposed PTC algorithms are shown in Fig. 10. From Figs. 7 and 8, it is notified that the proposed PTC operates at low switching frequencies. Hence, the switching frequency is reduced. Table 2 represents experimental steady-state torque and flux ripple of OEWIM drive. Torque and flux ripples are obtained with respect to their reference values.

5 Conclusions

This article provides basic idea to implement classical PTC to an OEWIM drive. This article suggests an improvised PTC algorithm for an OEWIM using normalised WSM. In classical PTC selection of weighting factor plays a vital role on performance of OEWIM drive. This article introduces a method to enhance the selection of weighting factors. The switching frequency involved in multi-level inversion fed OEWIM drives is too high. To address this problem, multi-objective cost function is formulated with the help of WSM to reduce switching frequency, torque and flux ripples. Classical PTC can reduce torque and flux ripples with high switching

Table 3 Parameters of OEWIM

Name	Symbol	Quantity
stator resistance	R_s	4.2 Ω
rotor resistance	R_r	2.6794 Ω
stator inductance	L_s	0.54 H
rotor inductance	L_r	0.54 H
mutual inductance	L_m	0.512 H
poles	P	4
inertia	J	0.031 kg-m^2
line-line voltage	V_{rms} (L–L)	400 V
rated power	P_{nom}	3.7 kW
torque	T_{nom}	24.48 N m
nominal/reference flux	ψ_{nom} or ψ_{sref}	1 Wb
nominal speed	N_r	1440 RPM
DC-link voltage	V_{dc}	540 V

frequencies. The proposed PTC can reduce torque, flux ripples and also significant reduction in switching frequency. Simulation and experimental results show the effectiveness of the proposed PTC algorithm. The proposed algorithm requires small increment in computational time, except that it gives all features and benefits of classical PTC.

6 References

[1] Takahashi, I., Noguchi, T.: 'A new quick-response and high efficiency control strategy of an induction motor', *IEEE Trans. Ind. Appl.*, 1986, **22**, (5), pp. 820–827

[2] Casadei, D., Profumo, F., Serra, G., *et al.*: 'FOC and DTC: two viable schemes for induction motors torque control', *IEEE Trans. Power Electron.*, 2002, **17**, pp. 779–787

[3] Buja, G.S., Kazmierkowski, M.P.: 'Direct torque control of PWM inverter-fed AC motors-a survey', *IEEE Trans. Ind. Electron.*, 2004, **51**, pp. 744–757

[4] Rodriguez, J., Cortes, P.: '*Predictive control of power converters and electrical drives*' (John Wiley & Sons, 2012)

[5] Miranda, H., Cortés, P., Yuz, J.I., *et al.*: 'Predictive torque control of induction machines based on state-space models', *IEEE Trans. Ind. Electron.*, 2009, **56**, (6), pp. 1916–1924

[6] Habibullah, M., Lu, D.D.C., Xiao, D., *et al.*: 'A simplified finite-state predictive direct torque control for induction motor drive', *IEEE Trans. Ind. Electron.*, 2016, **63**, (6), pp. 3964–3975

[7] Correa, P., Pacas, M., Rodriguez, J.: 'Predictive torque control for inverter-fed induction machines', *IEEE Trans. Ind. Electron.*, 2007, **54**, (2), pp. 1073–1079

[8] Geyer, T., Papafotiou, G., Morrari, M.: 'Model predictive direct torque control—part I: concept, algorithm and analysis', *IEEE Trans. Ind. Electron.*, 2009, **56**, (6), pp. 1894–1905

[9] Papafotiou, G., Kley, J., Papadopoulos, K.G., *et al.*: 'Model predictive direct torque control—part II: implementation and experimental evaluation', *IEEE Trans. Ind. Electron.*, 2009, **56**, (6), pp. 1906–1915

[10] Zhang, Y., Yang, H.: 'Model predictive torque control of induction motor drives with optimal duty cycle control', *IEEE Trans. Power Electron.*, 2014, **29**, (12), pp. 6593–6603

[11] Karamanakos, P., Stolze, P., Kennel, R.M., *et al.*: 'Variable switching point predictive torque control of induction machines', *IEEE J. Emerg. Sel. Top. Power Electron.*, 2014, **2**, (2), pp. 285–295

[12] Zhang, Y., Yang, H.: 'Two-vector-Based model-predictive torque control without weighting factors for induction motor drives', *IEEE Trans. Power Electron.*, 2016, **31**, (2), pp. 1381–1390

[13] Zhang, Y., Yang, H.: 'Generalized two-vector-based model-predictive torque control of induction motor drives', *IEEE Trans. Power Electron.*, 2015, **30**, (7), pp. 3818–3829

[14] Davari, S.A.: 'Predictive direct angle control of induction motor', *IEEE Trans. Ind. Electron.*, 2016, **63**, (8), pp. 5276–5284

[15] Habibullah, M., Lu, D.D.-C., Xiao, D., *et al.*: 'Predictive torque control of induction motor sensorless drive fed by a 3L-NPC inverter', *IEEE Trans. Ind. Inf.*, 2017, **13**, (1), pp. 60–70

[16] Rodriguez, J., Pontt, J., Silva, C., *et al.*: 'Predictive direct torque control of an induction machine'. Conf. Proc.: EPE-PEMC 2004 (Power Electronics and Motion control Conf.), Riga, Lativa, September 2004

[17] Zhang, Y., Yang, H., Xia, B.: 'Model predictive torque control of induction motor drives with reduced torque ripple', *IET Electr. Power Appl.*, 2015, **9**, (9), pp. 595–604

[18] Rodriguez, J., Kennel, R.M., Espinoza, J.R., *et al.*: 'High-performance control strategies for electrical drives: an experimental assessment', *IEEE Trans. Ind. Electron.*, 2012, **59**, (2), pp. 812–820

[19] Rojas, C.A., Rodríguez, J., Villarroel, F., *et al.*: 'Predictive torque and flux control without weighting factors', *IEEE Trans. Ind. Electron.*, 2013, **60**, (2), pp. 681–690

[20] Zhou, D., Zaho, J., Liu, Y.: 'Online tuning of weighting factors based on Sugeno-fuzzy method in predictive torque control of four-switch three-phase inverter-fed IM'. Int. Symp. Power Electronics, Electrical Drives, Automation and Motion, 2016, pp. 734–739

[21] Suresh, L., Nagarjun, S., Somasekhar, V.T.: 'Improvised SVPWM strategies for an enhanced performance for a four-level open-end winding induction motor drive', *IEEE Trans. Ind. Electron.*, 2017, **64**, (4), pp. 2750–2759

[22] Subotic, I., Bodo, N., Levi, E., *et al.*: 'On-board integrated battery charger for EVs using an asymmetrical nine-phase machine', *IEEE Trans. Ind. Electron.*, 2015, **62**, (5), pp. 3285–3295

[23] Kiadehi, A.D., Drissi, K.E.K., Pasquier, C.: 'Angular modulation of dual-inverter fed open-end motor for electrical vehicle applications', *IEEE Trans. Power Electron.*, 2016, **31**, (4), pp. 2980–2990

[24] Fernao Pires, V., Martins, J.F., Hao, C.: 'Dual-inverter for grid connected photovoltaic system: modeling and sliding mode control', *Sol. Energy*, 2012, **86**, (7), pp. 2106–2115

[25] Yao, Y., Cosic, A., Sadarangani, C.: 'Power factor improvement and dynamic performance of an induction machine with a novel concept of a converter-fed rotor', *IEEE Trans. Energy Convers.*, 2016, **31**, (2), pp. 769–775

[26] Jain, S., Ramulu, C., Padmanadhan, S., *et al.*: 'Dual MPPT algorithm for dual PV source fed open-end winding induction motor drive for pumping application', *Eng. Sci. Technol.*, 2016, **19**, (4), pp. 1771–1780

[27] Lu, S., Corzine, K.: 'Multilevel multi-phase propulsion drives'. Proc. IEEE Electric Ship Technologies Symp. (ESTS), Philadelphia, PA, July 2005, pp. 363–370

[28] Baiju, M.R., Gopakumar, K., Mohapatra, K.K., *et al.*: 'Five-level inverter voltage-space phasor generation for an open-end winding induction motor drive'. *IEE Proc. Electr. Power Appl.*, 2003, **150**, (5), pp. 531–538

[29] Praveen Kumar, K.V., Vinay Kumar, T.: 'Experimental implementation of direct torque control of open-end winding induction motor'. Conf. Proc.: IEEE TENCON-2016, 2016, pp. 3318–3323

[30] Kumar, A., Fernandes, B.G., Chatterjee, K.: 'Direct torque control of open-end winding induction motor drive using the concept of imaginary switching times for marine propulsion systems'. Conf. Proc.: IEEE PESC-04, 2004, vol. 2, pp. 1214–1219

[31] Praveen Kumar, K.V., Vinay Kumar, T.: 'Predictive torque control of open-End winding induction motor drive fed with multi-level inversion using two two-level inverters', *IET Electr. Power Appl.*, 2018, **12**, (1), pp. 54–62

[32] Zhu, B., Rajasekhara, K., Kubo, H.: 'Predictive torque control with zero-sequence current suppression for open-end winding induction machine'. Conf. Proc.: Industry Applications Society Annual Meeting, 2015, doi: 10.1109/IAS.2015.7356819

[33] Venugopal Reddy, B., Somasekhar, V.T., Kalyan, Y.: 'Decoupled space-vector PWM strategies for a four-level asymmetrical open-end winding induction motor drive with waveform symmetries', *IEEE Trans. Ind. Electron.*, 2011, **58**, (11), pp. 5130–5141

[34] Fishburn, P.C.: '*Additive utilities with incomplete product set: applications to priorities and assignments*' (Operations Research Society of America (ORSA), Baltimore, MD, USA, 1967)

[35] Triantaphyllou, E.: '*Multi-criteria decision making: a comparative study*' (Kluwer Academic Publishers (now Springer), Dordrecht, The Netherlands, 2000), p. 320. ISBN 0-7923-6607-7

[36] Krause, P.C, Wasynczuk, O., Sudhoff, S.D.: '*Analysis of electric machinery and drive systems*' (IEEE Press Power Engineering Series and Wiley-Interscience, Piscastaway, NJ, USA, 2002, 2nd edn.)

7 Appendix

7.1 Parameters of OEWIM

The parameters of OEWIM drive used in simulation and experimentation are shown in Table 3.

7.2 Estimation of stator flux

The stator flux of OEWIM drive is estimated by sensing DC-link voltages of inverter-1 (V_1) and inverter-2 (V_2). The total DC-link voltage is given by $V_{dc} = V_1 + V_2$. The total DC-link voltage has two functions: (i) it is used for the realisation of voltage space vectors in control algorithm and (ii) to estimate the phase voltages of OEWIM drive. From the total DC-link voltage, the phase voltages of OEWIM drive are estimated by using (4–(9). $V_{s\alpha}(k)$ and $V_{s\beta}(k)$ are obtained by applying Clarke's transformation to phase voltages ($V_{rr'}$, $V_{yy'}$ and $V_{bb'}$). The stator flux of OEWIM drive is obtained as

$$p\begin{bmatrix}\psi_{s\alpha}(k)\\ \psi_{s\beta}(k)\end{bmatrix}_m = \begin{bmatrix}V_{s\alpha}(k)\\ V_{s\beta}(k)\end{bmatrix}_m - R_s\begin{bmatrix}i_{s\alpha}(k)\\ i_{s\beta}(k)\end{bmatrix}_m \tag{35}$$

$$\begin{bmatrix}\psi_{s\alpha}(k)\\ \psi_{s\beta}(k)\end{bmatrix}_m = \int\left(\begin{bmatrix}V_{s\alpha}(k)\\ V_{s\beta}(k)\end{bmatrix}_m - R_s\begin{bmatrix}i_{s\alpha}(k)\\ i_{s\beta}(k)\end{bmatrix}_m\right)\mathrm{d}t \tag{36}$$